

Hidden Vela Supercluster Revealed by First Hybrid Redshift & Peculiar Velocity Reconstruction

A.M. Hollinger^{*1}, H.M. Courtois¹, R.C. Kraan-Korteweg², J. Mould^{3,4} and S.H.A. Rajohnson⁵

¹ Université Claude Bernard Lyon 1, IUF, IP2I Lyon, 4 rue Enrico Fermi, 69622 Villeurbanne, France

² Department of Astronomy, University of Cape Town, Private Bag X3, Rondebosch 7701, South Africa

³ Centre for Astrophysics & Supercomputing, Swinburne University, Hawthorn, VIC 3122, Australia

⁴ ARC Centre of Excellence for Dark Matter Particle Physics

⁵ INAF Osservatorio Astronomico di Cagliari, Via della Scienza 5, I-09047 Selargius, (CA), Italy

Received A&A March 7th, 2026; Accepted date:

ABSTRACT

A large fraction of the extragalactic sky is obscured by foreground dust and stars along the plane of the Milky Way, leaving a major gap ($\approx 20\%$) in whole-sky maps of large-scale structures, – an incompleteness that is even more severe for peculiar velocity samples. This has long limited an unambiguous interpretation of observed cosmic flows and their connection to the underlying mass-density field.

We present a new hybrid reconstruction methodology which combines 65,518 galaxy peculiar velocity distances from the CF4++ catalogue (Courtois et al. 2025) with 8283 new galaxy redshifts observed near the southern Galactic plane ($|b| \leq 10^\circ$) Zone of Avoidance. A major advance is the inclusion of 2176 high-sensitivity, interferometric HI redshifts obtained with the SARAO MeerKAT telescope which for the first time provide coverage of the innermost 3° -wide strip of the southern ZOA and to unprecedented depth.

This hybrid redshifts & peculiar velocities approach yields a substantially revised view of the inferred overdensities in and around the ZOA. In particular, the Vela supercluster emerges as a dominant mass concentration, rivaling the Shapley concentration and exceeding the mass associated with Laniakea and the Great Attractor region. With a total mass of $33.8 \times 10^{16} M_\odot$, a characteristic radius of $70 h^{-1} \text{Mpc}$, and a double core morphology at a distance of $189 h^{-1} \text{Mpc}$, Vela dominates the mass budget and gravitational influence of the southern Zone of Avoidance. These results provide the most complete and dynamically consistent picture to date of the southern Zone of Avoidance and demonstrate the transformative potential of hybrid reconstruction techniques tailored for the next generation of large-scale surveys.

Key words. Cosmology; large-scale structure of Universe

1. Introduction

Roughly a quarter of the extragalactic nearby Universe lies hidden behind the Milky Way, in what is commonly referred to as the Zone of Avoidance (ZOA). This obscured volume cannot be neglected when searching for potential deviations from ΛCDM or from General Relativity when studying the local cosmos: ignoring 25% of the volume risks biasing any inference on large-scale flows or density fields. However, obtaining galaxy distance measurements in this region is notoriously difficult, sometimes impossible, because galaxy images are heavily contaminated by the overwhelming number of foreground stars. This stellar crowding prevents reliable photometric parameter extraction. Moreover, corrections for Galactic foreground extinction add further uncertainties. Even in the K band, extinction is non-negligible close to the dust equator. An error in extinction of $A_K \sim 0.1$ mag translates into 200 km s^{-1} uncertainty in peculiar velocities, which precludes its use as standard distance indicators.

Despite these obstacles, galaxies in the ZOA can still be detected and positioned in redshift space with radio telescopes through the 21 cm line emission of neutral hydrogen gas (e.g. Staveley-Smith et al. 2016). With the advent of SKA Pathfinders, like the South African MeerKAT radio telescope and the

Australian SKA Pathfinder ASKAP, systematic interferometric HI-surveys are being pursued, such as WALLABY and DINGO Koribalski et al. (2020); Meyer (2009), respectively MIGHTEE-HI, FORNAX and LADUMA Maddox et al. (2021); Serra et al. (2016, 2023); Blyth et al. (2016) that allow significantly increased sensitivity, instantaneous redshift coverage, as well as positional accuracy compared to the earlier single-dish HI-surveys, and anchor these galaxies within the Hubble flow. After many years of data collection in South Africa, this work presents the first reconstruction of the obscured region using several thousands of galaxies, and marks the first time that a peculiar-velocity-based reconstruction (Courtois et al. 2012, 2023a, 2025) has been completed using a dataset that includes galaxies for which only redshifts - not distances - are available.

Developing and testing such a hybrid redshift & peculiar-velocity methodology is an essential preparation for the next generation of large surveys, which will simultaneously deliver both types of data over vast cosmic volumes. Projects such as DESI¹, 4MOST-4HS (Taylor et al. 2023), and WALLABY (Koribalski et al. 2020) are already beginning to assemble matched samples of redshift and velocity information, dramatically expanding the parameter space of future reconstructions. Establishing robust techniques that can integrate galaxies with full distance information together with those for which only redshifts

* amhollin@uwaterloo.ca

¹ www.legacysurvey.org

are available is therefore a crucial step. It ensures that forthcoming datasets can be exploited to their full potential, leading to more accurate maps of the local large-scale structure and more stringent tests of the Λ CDM model. Within the Λ CDM paradigm, large-scale structures emerge from the gravitational growth of initial density fluctuations dominated by cold dark matter, while cosmic acceleration is attributed to a cosmological constant Λ (Planck Collaboration et al. 2020a).

This paper is organised as follows. In Section 2 we summarise the datasets and methodology used to integrate the ZOA galaxies into the CF4++ catalogs within the Local Universe, adopted in this paper as $z < 0.1$, respectively $300 h^{-1}\text{Mpc}$. We present and discuss our results in Section 3, followed by our conclusions in Section 4.

2. Integration of ZOA velocity datasets to CF4++ database

In this section, we outline the different data sets compiled for this study. Our investigation concentrates on the southern ZOA, which hosts some of the most prominent over- and underdensities in the nearby Universe, including the Local Void (LV: Tully et al. 2008; Kraan-Korteweg et al. 2008), the Ophiuchus Supercluster (Oph: Hasegawa et al. 2000; Wakamatsu et al. 2005), the Great Attractor (GA: Dressler et al. 1987; Kraan-Korteweg et al. 1996; Woudt et al. 2004a), and the Vela Supercluster (VSCL: Kraan-Korteweg et al. 2017). To better characterise these structures and the flow fields they induce, numerous extensive, long-term galaxy surveys have been conducted. However, the paucity of ZOA data, particularly at higher redshifts where major contributions to the residual bulk flow are thought to arise, has remained a key concern. Recently, dedicated MeerKAT H I-surveys have delivered a substantial breakthrough by probing the innermost, fully opaque ZOA to unprecedented depths in sensitivity, angular resolution, and redshift range ($z < 0.085$), in addition to a number of spectroscopical surveys at intermediate ZOA latitudes.

The top panel of Fig. 1 displays the distribution in Galactic coordinates on the sky of the CF4++ together with the below presented ZOA redshift measurements, while the bottom panel provides a closer view of recent ZOA redshifts. The ZOA datasets are presented in four categories. The different symbols point to their respective sources and observations.

Dataset C1 (N=1096): contains H I-detected galaxies from the Parkes Multibeam ZOA survey (rms sensitivity of 6 mJy beam^{-1}), which was the first systematic HI survey of the southern ZOA specifically designed to trace obscured large-scale structures. HIZOA is composed of three components: the primary HIZOA catalog (HIZOA-S Staveley-Smith et al. 2016), a northern extension (HIZOA-NE Donley et al. 2005) covering $52^\circ > \ell > 196^\circ$ for $|b| < 5^\circ$, and a third extension targeting the Galactic Bulge (HIZOA-GB) (see Kraan-Korteweg et al. (2008), Kraan-Korteweg et al. in prep.), where stellar crowding and extinction extend to higher latitudes, covering latitudes $b = \pm 10^\circ$ for $332^\circ \leq \ell \leq 36^\circ$, and $b = +15^\circ$ for $348^\circ \leq \ell \leq 20^\circ$ (as indicated by red triangles around Galactic Bulge in bottom panel of Fig. 1). All three subsets were obtained with an identical instrumental configuration. The combined HIZOA survey sample consists of 1096 galaxies detected out to $cz \sim 12,700 \text{ km s}^{-1}$. Note though that the number of detections declines markedly beyond the distance range of the GA. Owing to the relatively large positional uncertainty (4 arcmin), cross-identification of sources—if visible in the ZOA—is particularly challenging.

Dataset C2 (N=4507): Optical spectroscopy in the Vela Supercluster region ($\ell = 272.5^\circ \pm 20^\circ, b = 0^\circ \leq \pm 10^\circ$). The extended Vela ZOA region has been a focus of interest for some time, as prominent, distant large-scale walls appear to vanish behind the ZOA, and early optical ZOA galaxy surveys had already revealed marked overdensities at similar distances (e.g. von Maltitz 2012). This motivated an extensive spectroscopic programme across the ZOA in 2012, targeting galaxies in areas where extinction and stellar confusion are still moderate. Redshift measurements were acquired using SpUpNIC on the 1.9m telescope (SAAO), the multi-object spectrograph (MOS) on the Southern African Large Telescope (SALT; Kraan-Korteweg et al. 2015) for candidate rich clusters, and – representing a substantial step forward – 25 fields observed with the 2dF+AAOmega spectrograph (392 fibres) on the 3.9m telescope of the Australian Astronomical Observatory (AAO). The latter yielded 4100 new, unique redshifts. When these are combined with earlier (unpublished) Vela redshift data obtained with the 6dF-MOS on the 1.2m Schmidt telescope at the AAO and with Optopus on the 3.6m telescope at ESO, the sample reaches 4432 redshifts in total (see Kraan-Korteweg et al. 2017). The recently reported 75 additional SALT redshifts in a rich VSCL cluster (Hatamkhani et al. 2024) contribute another 75 galaxies.

Dataset C3 (N=669): These measurements correspond to redshifts obtained via optical spectroscopy using the 6dF instrument on the 1.2m UK Schmidt Telescope at the AAO, collected during the early testing phase of the 6dF project. The 6dF pointings were situated within the ZOA ($|b| < 10^\circ$) and thus lay outside the main 6dF survey (Jones et al. 2009), from which the ZOA was excluded. Two supplementary programs were carried out: one targeted fields in the Puppis constellation – specifically, a strip spanning the full ZOA for $|b| < 10^\circ$ and centered at $\ell \sim 245^\circ$ – yielding 388 redshifts for 2MASX galaxies (Jarrett et al. 2000), 4 of these are listed in HIZOA, hence 384 new redshifts. The other focused on the Scorpius region near $\ell \sim 340^\circ$, providing an additional 285 redshifts (from optically identified and 2MASX galaxies), the majority of which lie at comparatively higher ZOA latitudes.

Dataset C4 (N=2825): This data sets summarizes the systematic H I-surveys that were undertaken in the southern ZOA. The observation were performed with the MeerKAT L-band receiver (856–1712MHz), and H I-data were extracted for the range 1308–1430MHz ($z < 0.085$, i.e. $cz < 25\,000 \text{ km s}^{-1}$), the volume within which RFI is minimal, while encompassing the full distance range relevant to (residual) bulk flows.

A first MeerKAT16 Science Verification experiment using the 16-dish subarray setup and the 32k ROACH correlator was carried out in May 2018 as a pilot study. It targeted six slightly overlapping pointings situated in a region of high galaxy density in Vela (around $(\ell, b) \sim (282^\circ, -8.3^\circ)$). The 3-hour observations achieved an rms noise level of $1.2 \text{ mJy beam}^{-1}$ and an excellent velocity resolution of 5.6 km s^{-1} at $z = 0$. A thorough examination of the resulting data products (Steyn 2023) yielded 119 robust detections (excluding 36 tentative galaxy candidates), 91 of which had no previously known redshifts in data set C2. The pilot survey thereby demonstrated that typical spiral galaxies can be readily detected out to the highest redshifts probed.

The success resulted in a proposal (led by RCKK) to exploit the then still ongoing SAAO MeerKAT Galactic Plane Survey (SMGPS Goedhart et al. 2024), a narrow survey of $|b| = 3^\circ$ along the Galactic Plane (~ 900 interleaving pointings of about 1 hr each aimed at continuum studies of the Galaxy) for a systematic H I-survey. The resulting H I data cubes led to an rms sensitivity of $0.3 - 0.6 \text{ mJy beam}^{-1}$, albeit with low velocity resolution

(44 km s⁻¹ at $z = 0$). The overall SMGPS H I-survey covered the longitude range from $260^\circ < \ell < 55^\circ$ for $z < 0.085$ ($cz < 25,000$ km s⁻¹). All data were reduced in a similar manner, (see e.g. Rajohnson et al. 2024a, for details on the data reduction and source extraction process). The analysis was divided into several sub-projects, each concentrating on specific-known or suspected-large-scale structures.

Kurapati et al. (2024) investigated the extended Local Void (LV), covering Galactic longitudes from $55^\circ > \ell > 332^\circ$ and constrained to $cz < 7500$ km s⁻¹ to encompass the full LV volume. They detected 291 galaxies in this region. These new detections substantially improved the mapping of the LV boundaries at these Galactic latitudes. A subsequent study analyzed the higher redshift range to uncover potential connections to the Ophiuchus supercluster unveiling an additional 431 galaxies (for early results, see Louw et al. (2026); Louw (2026), increasing the total to 722 H I-detections (30 in common with HIZOA). The adjoining SMGPS longitude range, $332^\circ > \ell > 302^\circ$, was surveyed to evaluate the prominence of the GA Wall as it cuts across the ZOA. Of the 477 galaxies detected there (42 already catalogued in HIZOA), nearly half trace an exceptionally pronounced wall at the distance of the GA (Steyn et al. 2024). The subsequent Crux SMGPS region was examined later to bridge the gap between GA and Vela, $302^\circ > \ell > 290^\circ$; the final assessment is still underway (see Steyn et al. 2026, for preliminary results). In this sector, 289 galaxies were detected (12 previously in HIZOA), revealing a so far unknown overdensity that may well be associated with the overall GA structure. In the SMGPS-VSCL longitude range, $290^\circ > \ell > 260^\circ$, the highest number of H I-detections was obtained (843 galaxies; 39 listed in HIZOA), tracing multiple large-scale structures at different distances, and a prominent peak at the distance of the Vela SCL (Rajohnson et al. 2024a).

The combined SMGPS H I-detections-eliminating duplicated in overlapping borders-yields a total 2288 H I-detections (112 of which are in HIZOA) hence 2176 are new redshift measurements. The total might still change slightly once the full SMGPS analysis has been completed.

A further H I-survey has been conducted with MeerKAT (Vela-HI; Rajohnson et al. 2024b) to extend the SMGPS to higher latitudes (about -6.7° to $+6.2^\circ$) over the longitude range $263^\circ \leq \ell \leq 284^\circ$ to trace the suspected connection of the Vela Walls seen in the optical spectroscopic surveys (see dataset C1), with those identified in the SMGPS (Rajohnson et al. 2024a). The set-up was similar, although the rms sensitivity was slightly lower, while the beam was slightly larger (see Rajohnson et al. 2024b, for details). A total of 719 galaxies were identified, of these 16 had an overlap with the above mentioned Vela-SMGPS, 79 of the remainder had HIZOA counterparts (C1), 66 had optical velocities (given in C2), leading to a sample of new redshifts of further sample of 558 new ZOA redshifts.

Taken the above described four data sets of 'southern' ZOA redshifts, from a total of 9092 unique redshifts, 8283 (at our cutoff at 30000 km s⁻¹) were added to the CF4++ catalog of 65518 galaxy distances. The coverage is displayed in Galactic coordinates in Fig. 1, where the top panel presents the merged CF4++ZOA survey. The sample now comprises 73801 individual galaxies. The bottom panel shows a close-up of southern ZOA data (red for H I and blue for optical redshifts). The power of the MeerKAT telescope in penetrating the innermost ZOA (C4: red circles), where little was known beforehand, is transformational.

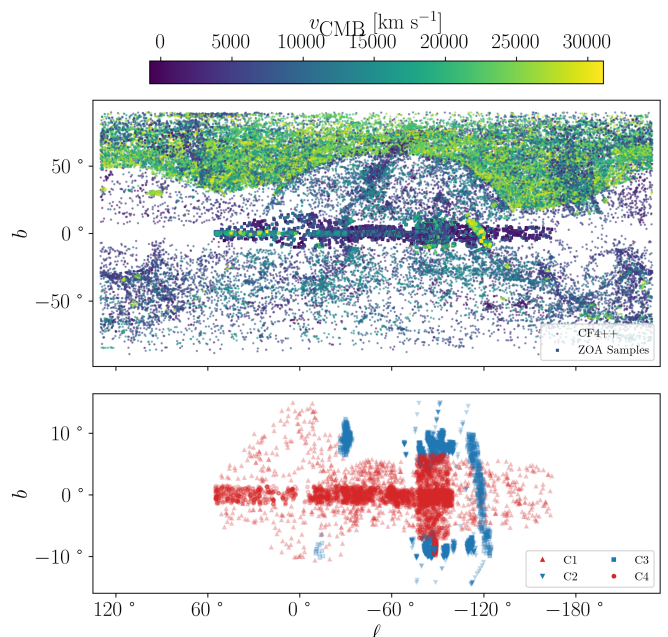


Fig. 1: The Galactic ℓ, b distribution of: (top) the CF4++ZOA samples along with their measured redshifts; and (bottom) the 8283 ZOA C1-C4 samples introduced in this work (red for H I and blue for optical redshifts). Note the unprecedented dense coverage provided by the seven datasets obtained with SARAO MeerKAT telescope (red circles) along the innermost, nearly fully opaque, ZOA region.

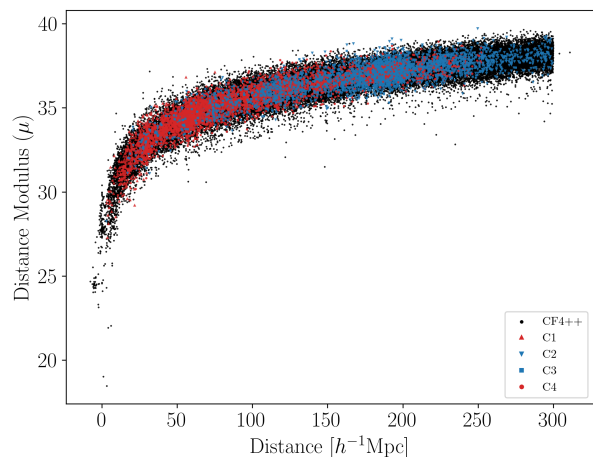


Fig. 2: Comparison of the CF4++ (black) distance moduli as a function of $V_{\text{CMB}}/100$ compared to the pseudo distance moduli adopted for the 8283 galaxies in the ZOA datasets (red for H I and blue for optical redshifts).

2.1. Test datasets

In order to verify that the hybrid reconstruction scheme does not produce artificial large scale structures, we computed a series of seven families of tests:

1. ZOA: distance moduli and peculiar velocities for ZOA galaxies are derived from the CF4++ data, to confirm that our new

reconstruction result in minimal changes compared to our previous reconstruction.

- (a) – *grid*: the peculiar velocity and uncertainties are assigned based on the CF4++ reconstruction grid, this results in distance moduli and uncertainties that exhibit significantly less scatter than the final ZOA C1–C4 galaxy samples,
 - (b) – *nearest*: assigns these quantities using the values of the nearest galaxy in the CF++ catalogue directly.
2. **MDPL2**: galaxy positions and peculiar velocities are taken directly from a mock catalogue, drawn from the MultiDark Planck 2 (MDPL2) simulation (see Appendix B for more details). These cases were performed to demonstrate that the reconstruction will not find non-existent structure and that we can test the robustness of the final results.
 - (a) – *area*: setup reproduces the radial selection function of the C1–C4 catalogs, while applying approximate Galactic latitude limits of 7.5° and 12° depending on their Galactic longitude, see Fig. 1. In this case, longitudes are assigned randomly.
 - (b) – *matching*., in contrast reproduces the radial selection function and matches the distributions of Galactic coordinates and object counts.
 3. **Random**: this variant uses a catalogue of randomly generated positions and velocities. Similar to the MDPL2 cases this ensures that assigning non-existent galaxies will not artificially introduce structure.
 - (a) – *area*: same as before,
 - (b) – *matching*: same as before,
 - (c) – *fully-random*: galaxy positions and distances are drawn entirely at random.

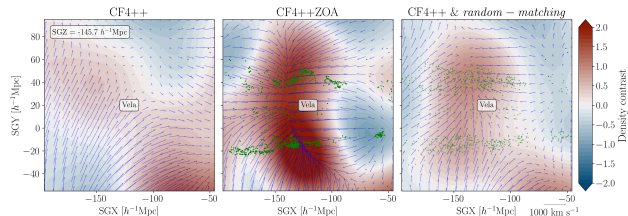


Fig. 3: Showing the differences in the Vela cosmography for the (left) CF4++, (middle) CF4++ZOA, (right) CF4++ & *random-matching* density reconstructions. The green points shown in the middle and right panels demonstrate the position of the artificial galaxies added, of the respective case.

Several tests were computed to check the robustness of the reconstructions. For example, Fig. 3 shows the Vela supercluster region for CF4++, CF4++ZOA and CF4++ & *random-matching*, the latter demonstrates the impact of adding an artificial dataset created with the same number of galaxies, located at the similar coordinates and depth as the ZOA observed galaxies, but assigned random peculiar velocities. Compared to the CF4++ density field both the ZOA and *random-matching* cases introduce a level of change to the local cosmography. However the random data does not introduce significantly larger density peaks than the original CF4++, nor changes to the overall velocity field when compared to the CF4++ZOA case. This clearly demonstrates that the reconstruction algorithm interprets this as white noise and that there is no significant correlation signal in this artificial dataset. Similarly, all seven tests confirm that the

hybrid reconstruction does not introduce spurious artifacts in either the density or velocity fields, nor generate artificial signals to the bulk flow (see Appendix for further details).

3. Results

In this section, we present an updated reconstruction of the Local Universe’s velocity and total matter (comprising both dark and luminous components) over-density fields, based on the hybrid model including the ZOA redshift data and compare these with the previous version of CF4++ (Courtois et al. 2025). The newly presented velocity fields are derived using a self-consistent approach, whereby the inferred field at any given point depends non-locally on the entire dataset. The methodology employed for these calculations aligns with the procedure detailed in Section 4 of Courtois et al. (2023b); for a more comprehensive explanation, we refer the reader to that paper.

3.1. Notable changes in reconstructed density and velocity fields

Substantial changes in the reconstructions based on the hybrid data set compared to the original CF4++ were revealed for the Lepus-Columba and the Vela supercluster, while most other previously identified overdensities in CF4++ (see Appendix C) show only minor variations (at levels below $|\delta| < 0.2$). Interestingly, the latter include the Local Void, the Great Attractor, and the Ophiuchus supercluster of which a significant fraction is located behind the ZOA (see Fig. C.1).

Here, we will focus on the description of the overdensities whose reconstructed full matter density and velocity fields were transformed quite radically. Figure 4 displays the original CF4++ dataset, the CF4++ZOA dataset, and their difference in the left, middle and right column respectively of a SGZ slice of $23.4 h^{-1} \text{Mpc}$ width which contains both Columba-Lepus and Vela (top and bottom, respectively). The CF4++ galaxies are marked by black dots, while the newly incorporated ZOA data points are shown as green dots. The changes in the shape, density and extent of these structures due to the addition of the ZOA datasets are significant and changes their local cosmography dramatically.

Columba-Lepus: Columba-Lepus is not located in the ZOA itself, but lies below the Galactic Plane at a lower distance compared to Vela. While it was recognised as a conglomeration of clusters (see the two density concentrations in the left panel), possible supercluster (see Fig. 4 in Pomarède et al. 2020), it now emerges as a strong oblong, elongated structure, more like a ridge, forming part of the boundary of a previously unknown, newly identified cosmic void expanding visibly into the ZOA at $\text{SGX,SGY}=(75; 0) h^{-1} \text{Mpc}$. The highest density core being Columba not Lepus.

Vela: Vela is significantly more prominent than in the previous reconstruction using only CF4++ dataset. It reveals two quite distinct prominent cores, embedded in a much larger structure. While this could be influenced by the distribution in the ZOA redshift dataset, various other galaxies are also observed between these two density peaks (see also bottom panel of Fig. 1). Moreover, such an effect has not been observed in other ZOA structures, like Local Void, Great Attractor and Ophiuchus, where the ample ZOA data resulted in marginal changes to the density field only; see Fig. C.1.

Near Vela, the velocity field is overall drastically modified and exhibits clear infall and backfall patterns around

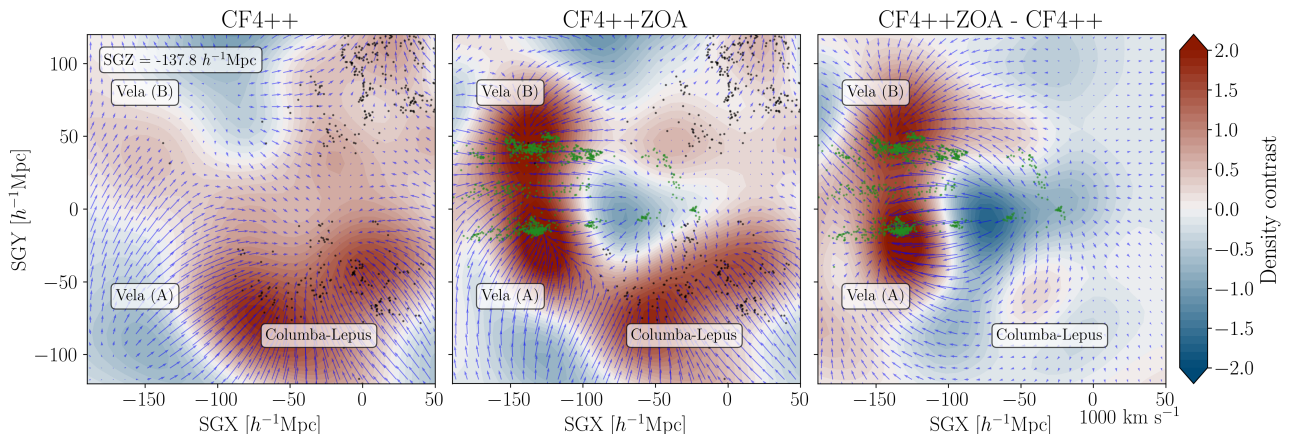


Fig. 4: The reconstructed matter density field, averaged over a total width of $23.4 h^{-1}\text{Mpc}$ in the SGZ plane of the superclusters regions that demonstrate the biggest changes with the addition of the ZOA datasets: Columba-Lepus and Vela. The left panel displays results derived from the CF4++ dataset, while the middle panel uses the CF4++ZOA dataset, and the right panel shows the difference between the two reconstructions. Overlaid is the mean velocity field. Black dots represent CF4++ galaxies, and the green dots correspond to newly added ZOA data points located within the averaged region.

the extended Vela supercluster. The localization of each Vela supercluster core is at supergalactic coordinates $(\text{SGX}, \text{SGY}, \text{SGZ}) = (-121.1, -19.5, -144.5) h^{-1}\text{Mpc}$ for Core *a* and $(-136.7, 50.8, -121.1) h^{-1}\text{Mpc}$ for Core *b*. The velocity plots favour Core *a* as the more prominent.

The two cores are separated by $75 h^{-1}\text{Mpc}$. Core *a* is slightly more massive with $14.4(3.7) \times 10^{16} M_{\odot}$ while Core *b* has $13.7(3.3) \times 10^{16} M_{\odot}$. Just as in Table 1, the mass in bracket is the central mass enclosed within the isocontour $\delta = 1.5$. The gravitational escape velocity from the cores is 4900 km s^{-1} compared to the Hubble expansion velocity of 3750 km s^{-1} between the two cores. That implies that Vela is still collapsing in comobile coordinates.

In Fig. 5, the reconstructed Vela supercluster is displayed together with other major superclusters of the Local Universe recovered from the CF4++ peculiar velocities reconstructions (Shapley, Hercules, Columba-Lepus, Apus, Pisces, Perseus, Laniakea, Coma). A streamline of the velocity field represents the spatial integral of the velocity field at a given time, tracing the instantaneous direction of motion through space rather than the time evolution of individual particles. Watersheds are then defined as the volumes that collect all streamlines converging toward the same attractor. When the flow crosses a cosmic void or becomes divergent, streamlines separate, and these regions of divergence define the ridge lines that form the boundaries between neighbouring watersheds. Figure 5 and Fig. 6 show that Vela indeed is a single gravitational watershed entity, with a double core that crosses and extends beyond the Galactic plane.

Isocontours of the density field provide a powerful tool to identify both the shape and the volume that define the boundaries of a supercluster. By selecting fixed thresholds of the density contrast δ , one can delineate regions of coherent overdensity and distinguish them from the surrounding large-scale structure. In our analysis (see Fig. 6) we show the isocontour levels corresponding to $\delta = 1.5, 2$ and 2.3 , where $\delta = 0$ corresponds to the cosmic mean density. Positive values of δ trace overdense structures, while negative values would identify cosmic voids. The isocontour at $\delta = 1.5$, encloses a very large and contiguous volume associated with the Vela supercluster, while the isocontours

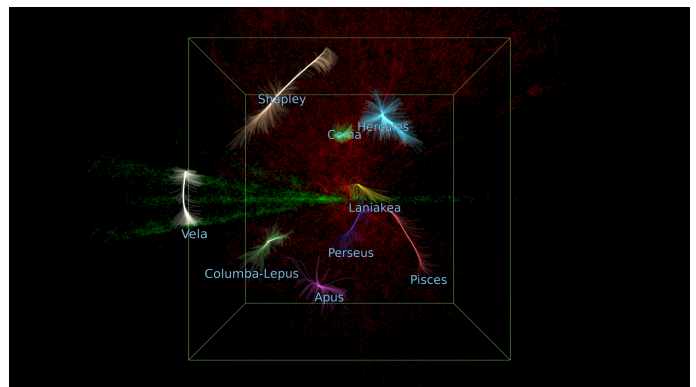


Fig. 5: Local superclusters reconstructed using the CF4++ dataset (red dots) expanded by the ZOA dataset (green dots). The green cube provides the $300 h^{-1}\text{Mpc}$ scale length and delineates the orientation primarily showing the SGX-SGY plane with +SGZ pointing forwards. Streamlines of the velocity field are coloured according to their gravitational watershed membership. The Vela supercluster emerges as a large single entity gravitational watershed on the left of the image, crossing the ZOA.

at $\delta = 2$ and $\delta = 2.3$ reveal the double core structure of Vela. Moreover, Fig. 6 outlines and defines its spatial extent and total enclosed volume geometrically, providing further evidence that the Vela structure extends well beyond the Galactic plane.

3.2. Dynamical masses of 8 nearby superclusters

In this subsection we will compute masses and typical radii of the main large scale structures for comparison of their respective parameters.

When the full three-dimensional velocity field $\mathbf{v}(\mathbf{r})$ is available, such as from detailed cosmological simulations or in this case reconstructed from observational peculiar velocity datasets, it becomes possible to estimate the mass enclosed within a spherical volume of radius R using the principles of linear theory. The process begins by calculating the divergence of the velocity field,

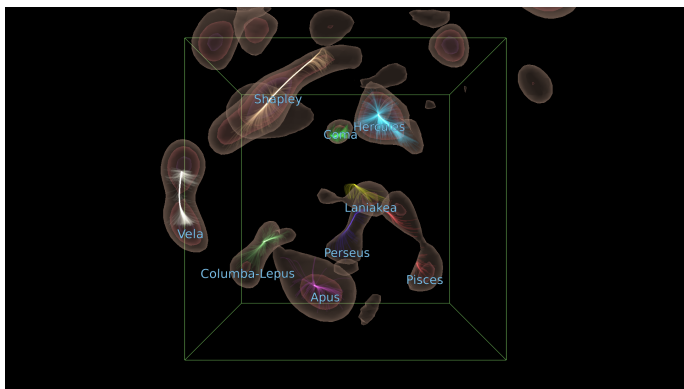


Fig. 6: The streamlines and layout are the same as in Fig. 5, with the addition of the iso-surfaces of the reconstructed density field in the Local Universe. The threshold delta field values for each isocontour is 1.5, 2 and 2.3. The Vela supercluster extends well beyond the Galactic plane with its internal structure showing a double core.

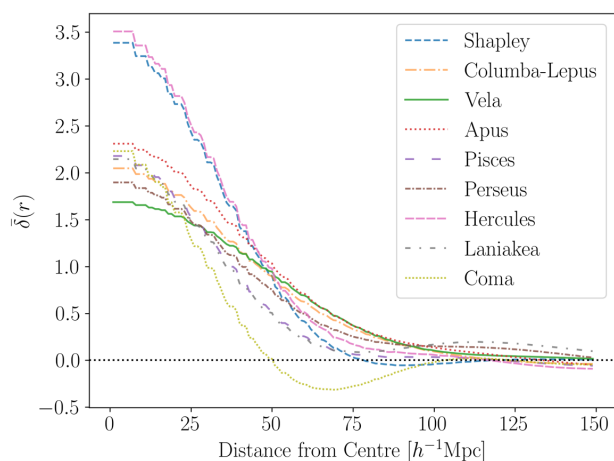


Fig. 7: The mean density profile of the local supercluster watersheds as a function of distance from their centre. The majority of these superclusters attain the average cosmic density at distances of $\sim 70 h^{-1}\text{Mpc}$ from their centres.

which quantifies how much the velocity field converges or diverges at each point in space. This divergence is then related to the density contrast $\delta(\mathbf{r})$ through the linear continuity equation, expressed as:

$$\delta(\mathbf{r}) = -\frac{\nabla \cdot \mathbf{v}(\mathbf{r})}{fH}, \quad (1)$$

where f is the linear growth rate of cosmic structures and H is the Hubble Constant. By integrating this density contrast over the spherical volume, specifically, summing contributions within the sphere the total enclosed mass can be estimated, such that:

$$M(< R) = \bar{\rho} \int_{|r|<R} (1 + \delta(\mathbf{r})) d^3r. \quad (2)$$

As the data are discretized into voxels, this integral is performed numerically by summing over all voxels within the sphere, multiplying the volume of each voxel by the local density contrast.

Here, $\bar{\rho}$ represents the mean matter density of the universe, serving as a baseline for the density fluctuations, with

$$\bar{\rho} = \frac{3H_0^2\Omega_m}{8\pi G} \approx 4.63 \times 10^{10} \text{ M}_\odot \text{ Mpc}^{-3}.$$

To accurately calculate the mass of these structures we first need to isolate each individual supercluster region. We use the density grid to identify all local maxima. We impose a minimum spatial separation of $20 h^{-1}\text{Mpc}$ between any two maxima to enforce realistic separations between supercluster domains. Secondly, a minimum threshold of the density contrast between two adjacent local minima is prescribed. These requirements ensure that each maximum represents a genuinely distinct physical region, preventing us from counting multiple peaks that merely trace the same underlying structure.

Once these maxima have been selected, we use each one as a seed for a flood-fill algorithm of the grid: during each step of this procedure, the regions associated with each seed are expanded outward by one layer of neighbouring grid cells, progressively 'filling' the superclusters starting from their central peaks. As the regions grow, we assign and maintain unique group identifiers for each supercluster, so that the emerging structures remain clearly distinguished throughout the process.

Figure 8 provides a comparative visualization between different methods of cosmic structure classification. The top panels display the density contrast maps, highlighting regions of varying matter density. The middle panels show the V-web classification, which delineates the cosmic web into voids, sheets, filaments, and knots based on velocity shear (see Section 3 of Hollinger & Courtois in prep. for details). The bottom panels present the final structure groupings, identifying the prominent superclusters using the method outlined above. Vela – which forms part of the structures in the left column – consistently exhibits a large density contrast with a split into two cores clearly evident when classified using the V-web technique.

Even though superclusters are not spherical, their integrated volumes can be used to compare typical radii. If we were to assume they were spheres, Vela has a typical radius of $70 h^{-1}\text{Mpc}$, Shapley $78 h^{-1}\text{Mpc}$ and Laniakea $58 h^{-1}\text{Mpc}$ (see Table 1). There is an alternative way of defining a typical radius of a supercluster which is to find the distance from the center that reaches the homogeneity of the Local Universe, i.e. where the δ field is zero. Figure 7 shows the mean mass density profiles of nearby superclusters. While the majority of these superclusters attain the average cosmic density at distances of $\sim 70\text{--}80 h^{-1}\text{Mpc}$ from their centres, they have significantly different density profiles. The Coma cluster or supercluster is the smallest among the local superclusters. Both the Shapley and Hercules superclusters display steep density profiles, indicating a rapid increase in density toward their cores. In contrast, the Vela supercluster is significantly more extended. With an estimated radius of about $100 h^{-1}\text{Mpc}$, it exhibits a more gradual, shallower density decline. Vela encompasses a total mass of $28.1 \times 10^{16} \text{ M}_\odot$, which is close to the mass of Shapley (83%) and almost 2 times the mass of Laniakea.

We indeed tested the method using a full $300 \text{ Mpc}/h$ MDPL2 mock catalog. For the examined simulated structures, the masses estimated within the defined "supercluster region" – using the density contrast δ and the fill algorithm – agreed with the true halo masses to within approximately 10%, which we thus consider as our error bar.

The escape velocity of a sphere of volume $14.7 \times 10^5 (h^{-1}\text{Mpc})^3$ and mass $28.1 \times 10^{16} \text{ M}_\odot$ is 5056 km s^{-1} . At

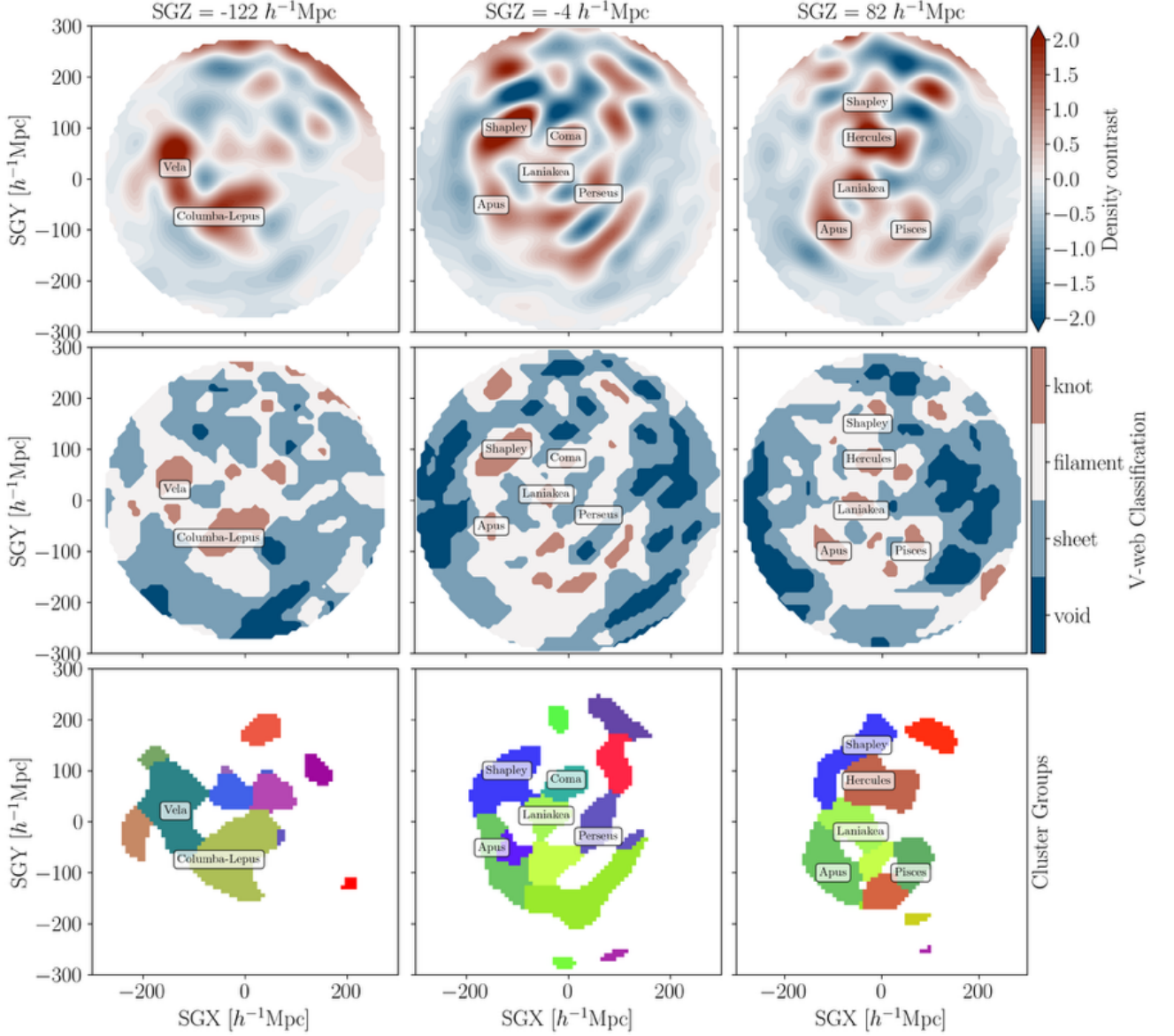


Fig. 8: Comparison of the density contrast (top row) to the V-web classification (middle row) to final structure groupings (bottom row). The left column shows a plane at $SGZ = -122 h^{-1} \text{Mpc}$, revealing the prominence of the Vela and Columba-Lepus superclusters; in the plane centered on $SGZ = 4 h^{-1} \text{Mpc}$ (middle column) Shapley, Coma, and Apus are most prominent; while in the plane centered on $SGZ = 82 h^{-1} \text{Mpc}$ (right column) Hercules, Pisces and Laniakea feature.

this radius, the Hubble expansion for Vela is about 7055 km s^{-1} assuming $H_0 = 74.6 \text{ km s}^{-1} \text{Mpc}^{-1}$. Thus at the furthest edge of Vela, such an idealized sphere's gravity dominates over cosmic expansion (see appendix for the details on computing these velocities in the proper comoving units).

We can also restrict this to the substructures Vela *a* and Vela *b* within the isocontour of $\delta > 1.5$: the escape velocity of a sphere of volume $2.1 \times 10^5 (h^{-1} \text{Mpc})^3$ and mass $7 \times 10^{16} M_\odot$ will then be 3490 km s^{-1} , while the expansion velocity at this radius is 3688 km s^{-1} . Thus expansion and gravitation are almost at the

equilibrium within this isocontour, where such an idealized object would be gravitationally bound in this simplified Newtonian picture. Shapley presents a similar case of a large scale structure largely expanding at its furthest isocontour while it is almost bound within the isocontour 1.5 in density contrast, at the current age of the Universe.

The inner part of Laniakea and Coma, the smallest local superclusters is close to the turnaround radius.

We find that the supercluster typical masses enclosed within the $\delta = 0$ isocontour are nearly an order of magnitude larger than

	ℓ, b , Distance $^{\circ}, ^{\circ}, h_{100}^{-1} \text{Mpc}$	SGX,SGY,SGZ $h_{100}^{-1} \text{Mpc}$	Mass $10^{16} M_{\odot}$	Volume $10^5 h_{100}^{-3} \text{Mpc}^3$	Escape vel. km s^{-1}	Hubble exp. km s^{-1}
Shapley	312, 48, 149	-98, 113, 4 (-106, 114, 3)	33.8 (10.1)	19.9 (3.0)	5272 (3951)	7804 (4154)
Vela	266, 1, 189	-121, -20, -145 (-122, -11, -161)	28.1 (7.0)	14.7 (2.1)	5056 (3490)	7055 (3688)
Hercules	27, 46, 113	-27, 74, 82 (-27, 74, 82)	17.0 (5.8)	7.9 (1.7)	4362 (3291)	5736 (3437)
Columba-Lepus	250, -33, 157	-51, -74, -129 (-59, -74, -122)	35.7 (4.4)	19.6 (1.5)	5432 (2927)	7765 (3297)
Apus	350, -35, 155	-105, -98, 59 (-106, -98, 66)	33.3 (4.0)	18.4 (1.3)	5302 (2858)	7603 (3143)
Pisces	98, -44, 133	74, -98, 51 (74, -89, 59)	16.7 (2.9)	8.6 (1.0)	4262 (2542)	5900 (2880)
Perseus	178, -39, 102	59, -59, -59 (66, -51, -59)	19.6 (1.9)	10.5 (0.7)	4466 (2184)	6306 (2557)
Laniakea	332, 6, 44	-43, -12, 74 (-43, -3, 82)	15.0 (1.5)	8.4 (0.5)	4055 (2052)	5854 (2286)
Coma	265, 85, 82	-4, 82, 4 (19, 82, -27)	6.2 (0.9)	3.3 (0.3)	3047 (1731)	4288 (1928)

Table 1: Listed are Galactic coordinates and distance, Supergalactic cartesian coordinates, mass, volume, escape velocity and Hubble expansion velocity of eight Local Universe superclusters, ordered by decreasing central mass. The coordinates SGX,SGY,SGZ correspond to the highest peak location in the density contrast field and in cosmic V-web for the values in brackets. The masses in the table assume $H_0 = 74.6$, the volume is just the number of voxels $\times (1000/128)^3$. Mass and volume values correspond to the full volume enclosed within the isocontour of homogeneity ($\delta = 0$). The value in brackets correspond to the center of the supercluster for which the local density contrast values are above 1.5. Vela is a close second in mass and extent to Shapley. It is similar to Hercules in mass but much more extended. None of the superclusters are gravitationally bound at their outermost boundaries where the typical difference between gravitational escape velocity and Hubble space expansion is of the order of 2000 km s^{-1} . Close to their centers, at the isocontour of $\delta = 1.5$ that difference is of the order of 250 km s^{-1} .

those reported in the review by Einasto (2025) and references therein, but the masses enclosed within the isocontour $\delta > 1.5$ are comparable. This discrepancy likely arises from methodological differences since most existing superclusters mass estimates rely primarily on luminosity-based methods rather than analyses of the underlying density or velocity fields. The discrepancies could also stem from differences in the definitions of the system’s spatial extent, and therefore its total mass. For example Shapley’s frequently cited value of $5 \times 10^{16} M_{\odot}$ attributed to Prout et al. (2006), appears to be based on an order-of-magnitude estimate. Despite these methodological differences, the two approaches yield results that are broadly consistent and mutually supportive, since we find $10.1 \times 10^{16} M_{\odot}$ for the central region of Shapley.

3.3. Bulk flow

Figure 9 presents a comparison of the amplitude (top panel) and direction (middle and bottom panels) of Local Universe bulk flow before (grey) and after adding the ZOA (blue) datasets. The CF4++ZOA reconstruction of the Local Universe velocity field is better constrained in Galactic longitude (ℓ), i.e., the variance is smaller. The direction of the bulk flow corresponds to the direction of Shapley and Vela at their respective distance, confirming that they are the main actors driving the local gravitational velocity field.

Compared to our previous reconstruction using CF4++ (Courtois et al. 2025), we see no significant changes in the amplitude of the bulk flow (see top panel of Fig.9), which is well constrained out to $250 h^{-1} \text{Mpc}$ with an amplitude of 400 km s^{-1} , well above what would be expected if the scale of homogeneity was reached at that distance (90 km s^{-1} in a ΛCDM prediction). This measurement is consistent with other measurements of the Local Universe inhomogeneity such as the DESI DR1 conditional density (Sylos Labini & Antal 2025).

Similarly there is minimal changes in the bulk flow direction in terms of Galactic latitude as a function of distance. However, we do see modest shifts in the Galactic longitude direction of the bulk flow at $\sim 50 h^{-1} \text{Mpc}$ and $\sim 190 h^{-1} \text{Mpc}$. With the bulk flow now remaining almost constant at $\ell \approx 280^{\circ}$ out to $175 h^{-1} \text{Mpc}$.

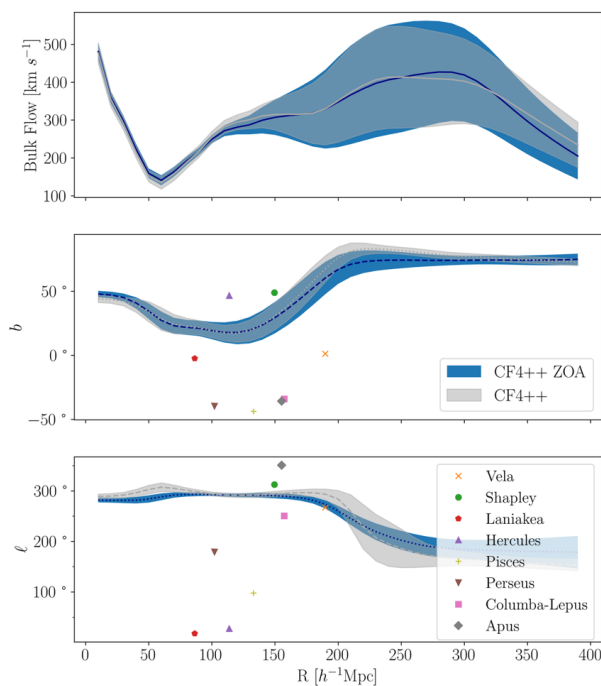


Fig. 9: Comparison of the amplitude (top) and Galactic b (middle) and ℓ (bottom) directions of the Local Universe bulk flow before (grey) and after adding the ZOA (blue) datasets. The mean and standard deviation (transparent bands) are calculated using the nearly 10,000 HMC realizations. The Galactic positions of the superclusters can be compared to the bulk flow direction.

4. Conclusions

This article reveals the double-core Vela supercluster, which is almost as massive as Shapley and twice more massive than La-

niakea. It is very extended, with a radius of $70 h^{-1}\text{Mpc}$ (assuming a spherical radius for its mass) and suggest a connection to the lower redshift Columba-Lepus supercluster located below the ZOA. All local major superclusters in the Local Universe have expansion velocities larger than gravitational escape velocity at their outermost boundaries, but they are close to being gravitationally bound within the isosurface of density contrast of $\delta > 1.5$. The here presented updated reconstruction of the velocity and density fields delivers better characterizations of the regions enclosed by Norma but results only in marginal changes to the Local Void, Great Attractor and Ophiuchus. This new addition of southern hemisphere data does not reduce the bulk flow, which stays at about 400 km s^{-1} at $250 h^{-1}\text{Mpc}$ distance, which exceeds 3 times the amplitude that would be predicted for a ΛCDM universe (90 km s^{-1}), indicative of the *bulk flow tension* as discussed in works such as Bouillot et al. (2014).

Having demonstrated that this hybrid redshift & peculiar-velocity approach can be applied successfully to several thousand galaxies in one of the most challenging regions of the sky, the next step is to extend the methodology to the vastly larger samples that are now becoming available.

Surveys like DESI, 4MOST/4HS and Wallaby will provide hundreds of thousands of redshifts alongside similarly large sets of peculiar-velocity measurements, and fully harnessing these datasets will require reconstruction techniques capable of handling their scale and complexity. The work presented here shows that such an integrated framework is feasible; the task ahead is to generalize and refine it so that it can operate efficiently and reliably on the much richer data streams soon to be delivered by the new generation of cosmological surveys.

Data Availability

All the datasets that were used are already published by the observers, apart from the private communication ones that will be published separately by Kraan-Korteweg et al.. The reconstructed density and velocity fields are available as usual : at the website of H. M. Courtois <https://projets.ip2i.in2p3.fr/cosmicflows/> or upon request if specific help or computational resolution is wanted.

The simulated data used in this article are publicly available from the COSMOSIM database <https://www.cosmosim.org/>, with their respective publications cited in section B.1.

Acknowledgements. We thank Dr. Jérôme Leca from RSA Cosmos company in France for creating figures 5 and 6 and their associated animations presented in this article. The authors gratefully acknowledge A. Louw, N. Steyn and S. Kurapati as important contributors to the HI-ZOA datasets. We express our acknowledgement and respect for the use of the land in South Africa and Australia on which the telescopes that were used are located, and the communities and custodians of these lands; in this context, given the importance of the SARAO Meerkat data at lowest latitude in this endeavor, we introduce a locally inspired affectionate name for the VELA supercluster, "Vela-Banzi", a Xhosa language name meaning "revealing widely". HMC acknowledges support from the Institut Universitaire de France and from Centre National d'Etudes Spatiales (CNES), France. JM acknowledges support from ARC grant CE2100008. The MeerKAT telescope is operated by the South African Radio Astronomy Observatory, which is a facility of the NRF, an agency of the Department of Science and Innovation. The CosmoSim database used in this paper (MDPL2) is a service by the Leibniz-Institute for Astrophysics Potsdam (AIP). AI-assisted tools were employed to improve some wording and grammar.

References

Behroozi, P. S., Wechsler, R. H., & Wu, H.-Y. 2012, *ApJ*, 762, 109, publisher: The American Astronomical Society

- Behroozi, P. S., Wechsler, R. H., Wu, H.-Y., et al. 2013, *ApJ*, 763, 18, [_eprint: 1110.4370](#)
- Blyth, S., Baker, A. J., Holwerda, B., et al. 2016, in *MeerKAT Science: On the Pathway to the SKA*, 4
- Bouillot, V., Alimi, J.-M., & Germani, C. 2014, in *Springer Proceedings in Physics*, Vol. 145, *Springer Proceedings in Physics*, ed. B. G. Sidharth, M. Michelini, & L. Santi, 113
- Courtois, H. M., Dupuy, A., Guinet, D., et al. 2023a, *A&A*, 670, L15
- Courtois, H. M., Dupuy, A., Guinet, D., et al. 2023b, *A&A*, 670, L15
- Courtois, H. M., Hoffman, Y., Tully, R. B., & Gottlöber, S. 2012, *ApJ*, 744, 43
- Courtois, H. M., Mould, J., Hollinger, A. M., Dupuy, A., & Zhang, C. P. 2025, *A&A*, 701, A187
- Donley, J. L., Staveley-Smith, L., Kraan-Korteweg, R. C., et al. 2005, *AJ*, 129, 220
- Dressler, A., Lynden-Bell, D., Burstein, D., et al. 1987, *ApJ*, 313, 42
- Einasto, M. 2025, *Universe*, 11, 167
- Goedhart, S., Cotton, W. D., Camilo, F., et al. 2024, *MNRAS*, 531, 649
- Hasegawa, T., Wakamatsu, K.-i., Malkan, M., et al. 2000, *MNRAS*, 316, 326
- Hatamkhani, N., Kraan-Korteweg, R. C., Blyth, S. L., & Skelton, R. E. 2024, *ApJ*, 972, 57
- Jarrett, T.-H., Chester, T., Cutri, R., et al. 2000, *AJ*, 120, 298
- Jones, D. H., Read, M. A., Saunders, W., et al. 2009, *MNRAS*, 399, 683
- Klypin, A., Yepes, G., Gottlöber, S., Prada, F., & Heß, S. 2016, *MNRAS*, 457, 4340
- Koribalski, B. S., Staveley-Smith, L., Westmeier, T., et al. 2020, *Ap&SS*, 365, 118
- Kraan-Korteweg, R. C., Cluver, M. E., Bilicki, M., et al. 2017, *MNRAS*, 466, L29
- Kraan-Korteweg, R. C., Jarrett, T. H., Elagali, A., et al. 2015, in *SALT Science Conference 2015 (SSC2015)*, ed. D. Buckley & A. Schroeder, 40
- Kraan-Korteweg, R. C., Shafi, N., Koribalski, B. S., et al. 2008, in *Astrophysics and Space Science Proceedings*, Vol. 5, *Galaxies in the Local Volume*, ed. H. Jerjen & B. S. Koribalski, 13
- Kraan-Korteweg, R. C., Woudt, P. A., Cayatte, V., et al. 1996, *Nature*, 379, 519
- Kurapati, S., Kraan-Korteweg, R. C., Pisano, D. J., et al. 2024, *MNRAS*, 528, 542
- Louw, A. 2026, Master's thesis, University of Cape Town, South Africa
- Louw, A., Kurapati, S., Pisano, D., et al. 2026, in *IAU Symp. 392, Neutral Hydrogen in and around Galaxies in the SKA Era*, ed. D. P. et al. (Cambridge: Cambridge University Press), in press
- Maddox, N., Frank, B. S., Ponomareva, A. A., et al. 2021, *A&A*, 646, A35
- Meyer, M. 2009, *Exploring the HI Universe with ASKAP*
- Planck Collaboration, Aghanim, N., Akrami, Y., et al. 2020a, *A&A*, 641, A1, [_eprint: 1807.06205](#)
- Planck Collaboration, Aghanim, N., Akrami, Y., et al. 2020b, *A&A*, 641, A6, [_eprint: 1807.06209](#)
- Pomarède, D., Tully, R. B., Graziani, R., et al. 2020, *ApJ*, 897, 133
- Prout, D., Quintana, H., Carrasco, E. R., et al. 2006, *A&A*, 447, 133
- Rajohnson, S. H. A., Kraan-Korteweg, R. C., Chen, H., et al. 2024a, *MNRAS*, 531, 3486
- Rajohnson, S. H. A., Kraan-Korteweg, R. C., Frank, B. S., et al. 2024b, *MNRAS*, 535, 3429
- Serra, P., de Blok, W. J. G., Bryan, G. L., et al. 2016, in *MeerKAT Science: On the Pathway to the SKA*, 8
- Serra, P., Maccagni, F. M., Kleiner, D., et al. 2023, *A&A*, 673, A146
- Staveley-Smith, L., Kraan-Korteweg, R. C., Schröder, A. C., et al. 2016, *AJ*, 151, 52
- Steyn, N. 2023, Master's thesis, University of Cape Town, South Africa
- Steyn, N., Kraan-Korteweg, R., Rajohnson, S., Kurapati, S., & Louw, A. 2026, in *IAU Symp. 392, Neutral Hydrogen in and around Galaxies in the SKA Era*, ed. D. P. et al. (Cambridge: Cambridge University Press), in press
- Steyn, N., Kraan-Korteweg, R. C., Rajohnson, S. H. A., et al. 2024, *MNRAS*, 529, L88
- Sylos Labini, F. & Antal, T. 2025, *arXiv e-prints*, [arXiv:2511.21585](#)
- Taylor, E. N., Cluver, M., Bell, E., et al. 2023, *The Messenger*, 190, 46
- Tully, R. B., Shaya, E. J., Karachentsev, I. D., et al. 2008, *ApJ*, 676, 184
- von Maltitz, K. 2012, Master's thesis, University of Cape Town, South Africa
- Wakamatsu, K., Malkan, M. A., Nishida, M. T., et al. 2005, in *Astronomical Society of the Pacific Conference Series*, Vol. 329, *Nearby Large-Scale Structures and the Zone of Avoidance*, ed. A. P. Fairall & P. A. Woudt, 189
- Woudt, P. A., Kraan-Korteweg, R. C., Cayatte, V., Balkowski, C., & Felenbok, P. 2004a, *A&A*, 415, 9
- Woudt, P. A., Kraan-Korteweg, R. C., Cayatte, V., Balkowski, C., & Felenbok, P. 2004b, *A&A*, 415, 9
- Woudt, P. A., Kraan-Korteweg, R. C., Lucey, J., Fairall, A. P., & Moore, S. A. W. 2008, *MNRAS*, 383, 445

Appendix A: Computing gravitational escape velocity and Hubble expansion in comoving distances

This appendix details the calculations employed to estimate the gravitational escape velocity of galaxy superclusters and the Hubble expansion velocity at specified comoving radii, as summarized in Table 1. These estimates are grounded in the cosmological parameters and voxel-based density fields derived from the CF4++ reconstruction, which encompasses a cubic comoving volume of $(1000h_{100}^{-1}\text{Mpc})^3$, subdivided into 128^3 voxels. Consequently, each voxel has a linear size of $\ell = 7.8125 h_{100}^{-1}\text{Mpc}$, corresponding to a volume of $V_{\text{voxel}} = \ell^3 = 476.8 h_{100}^{-3}\text{Mpc}^3$.

Adopting a Hubble constant matching that of CF4++, i.e. $H_0 = 100h \text{ km s}^{-1}\text{Mpc}^{-1}$ with $h = 0.746$, and a matter density parameter $\Omega_m = 0.3$, the critical density is calculated as:

$$\rho_{\text{crit}} = 2.775 \times 10^{11} h^2 M_{\odot} \text{Mpc}^{-3} \approx 1.54 \times 10^{11} M_{\odot} \text{Mpc}^{-3}.$$

The physical size of each voxel is then approximately 10.47 Mpc, with a corresponding volume of $V_{\text{voxel}} = 1148.6\text{Mpc}^3$. The mean matter density follows as $\bar{\rho} = \Omega_m \rho_{\text{crit}}$, and the mass within a voxel with overdensity δ_i is

$$M_i = \bar{\rho}(1 + \delta_i)V_{\text{voxel}} \approx 1.77 \times 10^{14} \Omega_m (1 + \delta_i) M_{\odot}.$$

As an example, consider the Shapley supercluster which spans a volume of $V = 1.99 \times 10^6 h^{-3}\text{Mpc}^3$ and has a mass of $3.38 \times 10^{17} M_{\odot}$. Assuming spherical symmetry its radius can be estimated as $R = 4/3\pi R^3 \approx 78h^{-1}\text{Mpc} \approx 105 \text{ Mpc}$. The gravitational escape velocity at this radius is given by

$$v_{\text{esc}} = \sqrt{2GM/R} \approx 5300 \text{ km s}^{-1},$$

where $G = 4.302 \times 10^{-9} \text{Mpc} (\text{km s}^{-1})^2 M_{\odot}^{-1}$. The Hubble expansion velocity at this radius is

$$v_H = H_0 R \approx 7800 \text{ km s}^{-1}.$$

This comparison illustrates the interplay between the gravitational binding of the supercluster and the cosmic expansion at this scale.

Appendix B: Tests

Appendix B.1: MDPL2 mocks

We used the MultiDark Planck 2 (MDPL2) simulation, which is part of the MultiDark project, a set of cosmological hydrodynamic simulations (Klypin et al. 2016). All simulations in this suite adopt a flat Λ CDM cosmology with the following parameters: $\Omega_{\Lambda} = 0.692885$, $\Omega_M = 0.307115$, $h = 0.6777$, $\sigma_{8,\text{linear}} = 0.8228$, and $n_s = 0.96$, in agreement with the Planck measurements (Planck Collaboration et al. 2020b). MDPL2 follows 3840^3 dark matter particles, each with mass $1.51 \times 10^9 h^{-1}M_{\odot}$. Haloes were identified using Rockstar (Behroozi et al. 2012), which led to over 10^8 haloes. Halo merger trees were subsequently constructed with ConsistentTrees (Behroozi et al. 2013). The simulation volume is a periodic cube of side length $1000 h^{-1}\text{Mpc}$. Our analysis is restricted to the $z = 0$ snapshot. The halo catalogue was retrieved from the COSMOSIM database².

² www.cosmosim.org

We select a random region from the MDPL2 simulation, ensuring a volume of radius $300 h^{-1}\text{Mpc}$ to match the survey depth of CF4++. Within this region, we calculate the radial velocity of halos, using the Cartesian peculiar velocities provided, in the CMB frame with respect to the origin. To reflect the limitations inherent to observational surveys, we apply increasingly larger cuts in halo mass as a function of distance from the origin, starting from approximately $\sim 5 \times 10^9 M_{\odot}$ and increasing logarithmically up to $10^{12} M_{\odot}$ at $300 h^{-1}\text{Mpc}$. Additionally, we convert the positions of the halos to Galactic coordinates, and exclude all objects with $|b| > 15^\circ$ to isolate the Galactic plane region. The final selection of halos is determined following the criteria outlined in the previous section.

Appendix B.2: Description of Tests

To validate our methodology and ensure that we are not over-analyzing the dataset, we conduct three types of tests.

- The first tests (*ZOA*) uses the Zone of Avoidance C1-C4 samples and CF4++ datasets directly. Using both the catalogues and previous reconstructions to assign peculiar velocities and distance moduli our HMC reconstruction scheme. By design we expect these reconstructions to reproduce the original CF4++ density and velocity fields.
- The second set (*MDPL2*) involves introducing simulated data into the ZOA. We use the MDPL2 haloes directly for these tests as the actual luminosity of these objects is not important for our purposes. To maintain consistency, we also cut the number of simulated data down to include a most an equivalent number of galaxies as in the original sample, allowing us to assess the robustness of our analysis procedures under controlled conditions. As we expect the structure that our HMC finds to be coherent and match with the true density field that one would recover in the ZOA region.
- The third set (*random*) of tests produces data that is largely incoherent, with the only consistent aspect being the number of objects in the ZOA sample. In this test, the mock galaxies are randomly distributed within the ZOA, with their positions assigned arbitrarily. Their peculiar velocities are also assigned randomly, aligning with the distribution of the CF4++ sample. This approach results in a dataset that does not preserve the underlying spatial or kinematic correlations observed in the original sample.

In all cases, the uncertainties associated with the generated samples are computed following the methodology outlined in section 2.1.

Figure B.2 shows the changes to the density field through the Galactic plane ($b \approx 0^\circ$), for the CF4++ (left), test cases (middle) and difference between the two (right). As expected, the *ZOA* configurations – our first tests displayed in the top row – exhibit the smallest modifications in the reconstructed density field. This behaviour is expected, as we explicitly constrain the peculiar velocities of the added galaxies to be consistent with our earlier measurements.

In contrast, in the *fully-random* scenario (fourth row), the density field becomes systematically less extreme across all regions: previously under-dense regions become more populated, while over-dense regions are smoothed out and become less pronounced. As expected this trend is similarly observed in the *random-area* realizations, and to a lesser extent in the *random-matching* (third rows).

Unsurprisingly the *MDPL2-area* scenario (second row, left panel) generates the largest changes to the $b \approx 0$ plane. While the

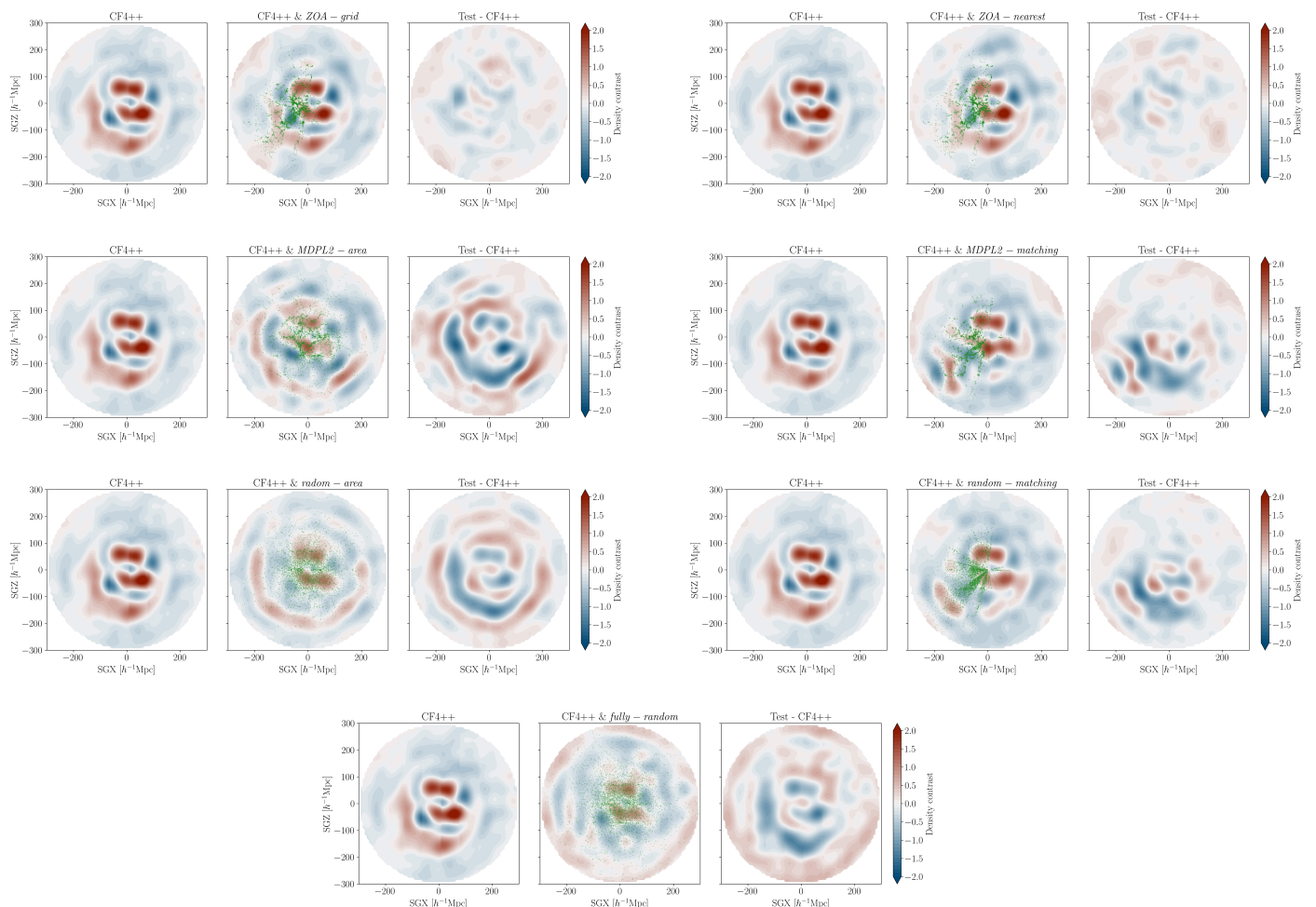


Fig. B.1: The local cosmography sliced through the Galactic plane ($b \approx 0^\circ$), the left and middle column show the mean of the HMC realizations of the density contrast (δ) for CF4++ and our test cases, respectively. The right column shows the difference between the two. The green points shown in the middle panel demonstrate the position of the artificial galaxies added, of each test case.

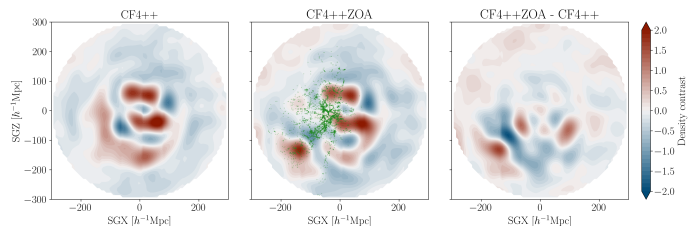


Fig. B.2: Similar to Fig. B.1 showing the CF4++&ZOA reconstruction presented in this work

peculiar velocities assigned to the random case effectively wipe out existing structure. The MDPL2 mock local universe has its own structures that do not directly correspond to our observed Local Universe. This thus introduces an additional mismatch when used to fill in the missing data. The *MDPL2-area* case also shows this general tendency (second row, right panel), but to a lesser extent. At the same time, it produces the largest overall discrepancies in the density field, reflecting the fact that the MDPL2 mock catalogues are not an exact representation of the actual Local Universe and thus introduce additional mismatch when used to fill in the missing data.

In all cases, none of the test scenarios exhibit density peaks in the Vela region that are as prominent or extensive as those observed in the CF4++ and ZOA C1-C4 case, as illustrated in Fig. B.2.

Appendix C: Reconstructions of other structures

We analyzed 31 well known large scale structures in the Local Universe: Antlia, Great Attractor, Lepus, Pisces, Aquarius, Great-Arch, Local Void, Sculptor, Arch-knot, Great-Attractor, Shapley, Bootes, Great-Wall, Norma, southern-Wall, Centaurus, Hercules, Ophiuchus, Ursa-Major, Columba, Hercules, Pavo-Indus, Vela, Coma, Horologium-Reticulum, Perseus-Pisces, Virgo, Corona Borealis, Hydra, Phoenix, Fornax, Leo, Pisces-Cetus. The majority of them show minimal to no changes in both their density and velocity fields.

Norma, Great Attractor, Local Void and Ophiuchus:

Figure C.1 shows four local large scale structures that were most likely to be affected by the inclusion of ZOA data due to their proximity to the Galactic plane, i.e. Norma, the Great Attractor, the Local Void or Ophiuchus. Interestingly, no dramatic change is notable in their local cosmography, apart from Norma whose shape is better defined with the inclusion of the ZOA datasets (see top row in Figure C1). It is separated from

neighbouring structures, exhibits a round morphology, and is well embedded within the Zone of Avoidance. Norma appears to lie along the wall of a cosmic void located just below it at $(-12; -50) h^{-1}\text{Mpc}$ in SGX-SGY. While a lack of data just behind the Norma cluster was already notable in (Woudt et al. 2004b, 2008) the actual extent –and roundness – of the void could not be defined with the previously existing data.

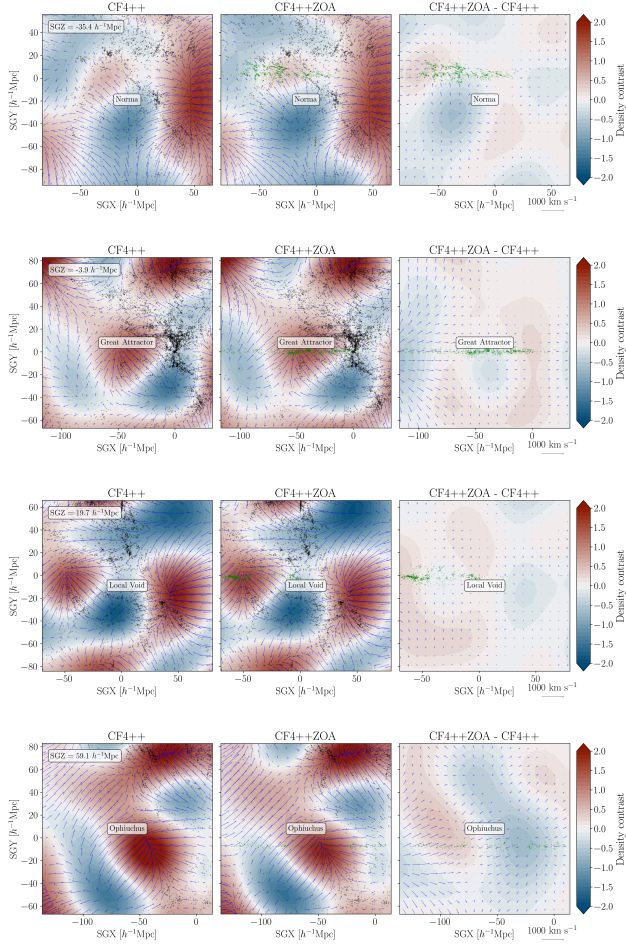


Fig. C.1: Similar to Fig.3, the reconstructed matter density field, averaged over a total width of $23.4 h^{-1}\text{Mpc}$ in the SGZ plane. The left panel displays results derived from the CF4++ dataset, while the middle panel uses the CF4++ZOA dataset, and the right panel shows the difference between the two reconstructions. Overlaid is the mean velocity field. Black dots represent CF4++ galaxies, and the green dots correspond to newly added ZOA data points located within the averaged region. The plots show four structures located near the Galactic plane that interestingly demonstrate no significant changes to their local cosmography although the addition of the ZOA datasets. From top to bottom these are Norma, Great Attractor, the Local Void and Ophiuchus.